Journal of Energy Storage 105 (2025) 114725

Contents lists available at ScienceDirect

Journal of Energy Storage

journal homepage: www.elsevier.com/locate/est

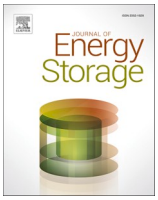

Research papers

Comparative study of methodologies for SOH diagnosis and forecast of LFP and NMC lithium batteries used in electric vehicles

F.A. Vásquez *, P. Sara Gaitán, Jorge A. Calderón *

Centro de Investigación, Innovación y Desarrollo de Materiales – CIDEMAT, Universidad de Antioquia, Cr. 53 No 61 – 30, Torre 2, Lab. 330, Medellín, Colombia

ARTICLE INFO

Keywords:
Second life
State of health
Diagnostic methodology
lithium battery
Electric mobility

ABSTRACT

The exponential growth of electric mobility requires alternatives to extend the life of batteries in new applications and reduce the environmental impact of retired lithium batteries. The second life is an economic and environment-friendly alternative for battery management. The development of fast, low-cost, and reliable diagnostic methodologies makes it possible to increase the economic benefits and reduce the remanufacturing time of second-life batteries (SLBs). In the present work, battery state of health (SOH) distribution analysis, incremental capacity (IC), internal resistance (IR), and electrochemical impedance spectroscopy (EIS) were applied as diagnostic methodologies for two different chemistries of lithium-ion batteries previously used in electric vehicles (EV). In addition, module equalization in batteries was done in order to assess whether the state of module charge (SOC) variation affects the SOH. The results demonstrate that the diagnosis methodology depends on the chemistry of the battery, and that there is no single reliable diagnostic procedure that can be applied to all types of lithium-ion batteries. It was determined that the most adequate diagnostic method for LFP batteries ($LiFePO_4$ cathode) is the IC method, while for NMC batteries ($LiNi_{0.33}Mn_{0.33}Co_{0.33}O_2$ cathode) the IR and EIS diagnostic methods are the most appropriate. Similarly, the present work proposed a simple methodology for IC capacity diagnosis and a general expression for SOH determination by IC and incremental voltage diagnosis of LFP batteries. Higher stability of LFP respect to NMC modules was observed during the SLBs performance, retaining >99 % after 500 cycles for LFP, compared with 90.2 % for NMC. The remaining useful life (RUL) shows that there are kinetics and lithium inventory changes in the batteries temperature-dependent.

1. Introduction

The use of EV has been growing during the last two decades as a consequence of greenhouse emission control policies. The global market is projected to grow from >9 million units in 2022 to >39 million units in 2030 [1]. Colombia reported 31 thousand electric and hybrid vehicles in 2023 [2], and is one of the current leaders of the EV market in Latin-America. The 5 EV with the most units sold in Colombia are Zhidou D2S (battery 18 kWh), BYD YUAN (battery 50.1 kWh), BYD IDOLPHIN (44.9 kWh), MINI Cooper (32.6kWh), and MAZDA MX-30 (35.5 kWh) [3]. The lithium battery average life is 7 years, which would correspond to >120 MWh of lithium batteries retired from EV available for second life application. The second-life batteries have at least 5 years of remaining life. SLBs can be a solution to store renewable energy. Additionally, the kWh cost of SLBs is lower (65 USD/ kWh) than new LIBs (209 USD/kHh) and lead acid batteries (100–200 USD/kWh) [4,5] The remanufacture of SLBs requires several processes to be implemented, including the dismantling of batteries, diagnosis of the SOH for modules or cells, and classification and reassembly of SLBs [6]. To reduce the process time and economic cost of SLBs diagnosis it is necessary to develop adequate testing methodologies to determine whether each individual cell or module is adequate for continued use in a second application for an energy storage system [7].

Batteries are constituted by easily dismantable modules, as the union is by screw or contact without welding unions. The modules are constituted by series and/or parallel cells configuration that are difficult and unsafe to dismantle with welding union. Although in other studies diagnosis was done by individual cells, obtaining a high correlation between indicators and SOH, the scaling up of the SLBs process by modules in which several cells in series and/or parallel were connected requires less time [7]. Studies have demonstrated that cells in series configuration show slight variations in SOC; these changes can affect the accuracy of diagnostic methodology [8].

* Corresponding authors.
E-mail addresses: ferley.vasquez@udea.edu.co (F.A. Vásquez), andres.calderon@udea.edu.co (J.A. Calderón).

https://doi.org/10.1016/j.est.2024.114725
Received 14 May 2024; Received in revised form 11 September 2024; Accepted 20 November 2024
Available online 27 November 2024

1.1. Methods of battery diagnosis

Battery degradation can take place due to several factors that affect SOH, such as loss of lithium inventory, lithium precipitation, electrolyte degradation, and chemical and structural changes in active materials of electrodes [9]. Several alternatives to calculate or estimate the SOH of a battery have been reported in the literature, such as the coulomb counting method (CCM), internal resistance (IR), incremental capacity (IC), efficiency of energetic utilization (EUE), voltage fluctuation (ΔU), average distance of Fréchet (ADF), and electrochemical impedance spectroscopy (EIS). CCM is one of the most useful and direct techniques used to calculate the SOH, however, it requires more time than other methods.

Internal resistance can be calculated according to Eq. (1). Also, internal resistance (IR) is made up of ohmic resistance and polarization resistance, as described by Eq. (2). Internal resistance depends on SOC and SOH; for this reason, to estimate SOH in modules or batteries with series or parallel cell configurations high equalization between cells is required (same SOC) in order to increase the SOH estimation accuracy [10].

$$IR = (Vocp - Vi)/I_{0.2C} \tag{1}$$

where "Vocp" is the open circuit potential (OCP), which depends on SOC and SOH of the component and "Vi" is the voltage when the current "$I_{0.2C}$" is applied. A current equivalent to 0.2C is recommended.

$$IR = Rohm + Rp \tag{2}$$

where "*Rohm*" is the ohmic resistance associated with electrolyte resistance and the resistance of electronic components and "*Rp*" is the polarization resistance, whose value is affected by the charge transfer resistance and the diffusion resistance of the cells. *IR* affects the voltage drop during discharge as described by Eq. (3), and therefore the energy density drops. The difference between charge and discharge voltage is called the hysteresis effect, and this effect depends on the *IR* [11].

$$Vdis = Vocp–Idis^{*}IR \tag{3}$$

where, "*Vdis*" is the voltage drop during discharge, "*Vocp*" is the open circuit voltage, "*Idis*" is the current during the discharge and "*IR*" is the internal resistance evaluated by Eq. (1) [8,12]. As can be seen from Eq. (3), discharge processes at high C-rates produce high voltage drops.

The real energy density is lower than the theoretical energy density as a consequence of the limitations of different cells, such as structural defects, voltage drops at high C-rates or partial structure lithiation-delithiation during the discharge-charge process under high C-rate conditions. The kinetics of charge/discharge processes in lithium batteries depend on factors such as electronic conductivity, ionic mobility, diffusion constants, the morphology of the active material and the possible presence of discontinuities. Additionally, during the calendar or cycle life of lithium-ion cells, some degradation processes can take place, generating a loss of active material, microcracks and resistive layers, which in turn slow the intercalation processes of the lithium ions and decrease electronic conductivity. The lithium content in the electrolyte can be reduced by the formation of compounds from side reactions on the active material, generating lithium-inventory reduction in the electrolyte. All these factors affect the capacity, the state of health (SOH) and the C-rate performance, and promote dendrite formation which short-circuits the electrodes [12]. The calendar life or cycle life is correlated with the SOH of batteries. Several aspects like chemical and structural features of active material, working temperature, overcharge or over-discharge events and prolonged storage periods of the batteries accelerate the degradation processes [13]. The degradation process causes capacity loss and C-rate drop during calendar and cycle life, depending on internal resistance increases, solid electrolyte interphase (SEI) growth, lithium inventory loss, and lixiviation of the active material, whose degradation rate increases with the temperature, C-rate and depth of discharge (DOD) [14]. The electrical parameter changes in the cathode, anode, electrolyte and diffusion process can be calculated by electrochemical impedance spectroscopy (EIS) [14,15].

The SOH is the percentage of nominal capacity that the battery, module, or cells retain after several days or cycles under operation. The SOC provides information about the current energy amount stored in the battery. State of charge (SOC) and state of health (SOH) are determined by CCM, as described by Eqs. (4) and (5), respectively [16]. The SOH determination is calculated conventionally by full charge-discharge cycle, and SOC can be calculated by the instantaneous current integral, as described in Eq. (4). Diagnostic accuracy of modules or batteries presents slight variation as a result of variations in SOH and SOC of cells in series or parallel cells; the cells show variations in their own internal resistance and EIS parameters, and the values are the average performance of all cells, obtaining a poor correlation between the electrical parameters and the SOH of the battery. Nevertheless, dismantling the batteries or modules in individual cells requires more time, is a dangerous process and increases the diagnostic cost.

$$SOC = \int_{to}^{t} \frac{IBat}{Nominal\ capacity^{*}SOH} dt + SOCini \tag{4}$$

$$SOH = \frac{Actual\ capacity}{Nominal\ capacity}{}^{*}100 \tag{5}$$

where, IBat is the instantaneous charge or discharge current applied to the battery, SOCini is the initial state of health charge of battery, and SOH is the initial state of health (conventionally set at 100 %). The CCM is the most applied diagnostic method given that prior calibration curves are not required. Nevertheless, Eq. (4) supposes both stable SOH and coulombic efficiency, disregarding their variation during cycle life. This induces a progressive error during the measurement. In addition, estimating the SOH and SOC by cell voltage, EIS, IR or artificial intelligence shows a high level of error given that the voltage measurement depends on the current applied during charge or discharge, as is described by Eq. (3). The artificial intelligence methodologies such as "average Fréchet distance" require a high amount of data, and there is high variation between the modules or cells [11].

Aging study by EIS is a fast diagnostic method; however, a deep understanding of the electrochemistry of the process involved is required to analyze the results and it is very sensitive to the SOC, obtaining a poor correlation with SOH as a consequence of unbalancing between cells or modules of the battery [15].

The incremental capacity (*IC*) diagnostic method studies the aging mechanism by the charge profile derivation as described in Eq. (6). The method identifies whether capacity is lost by lithium inventory, active material degradation, or kinetic changes [8,17]. The charge capacity derivation described in Eq. (6) can be obtained under constant current ($\Delta I = 0$), so the equation is simplified. This method is additive, and the total contribution is the sum of the contribution of series or parallel cells arrangement. This characterization method requires a calibration curve for each reference of module or battery [8,17]

$$IC = \frac{dQ}{dVk} = \frac{dQ}{dVocp + R\Delta I} = \frac{dQ}{dVocp} \tag{6}$$

Additional methods estimate the current capacity or the capacity lost by the imbalance or ohmic drops between cells in series configuration. Energy utilization efficiency (EUE) evaluates the SOC equalization degree of modules or cells to estimate the current capacity of the battery. It also evaluates the effect of cell aging on the SOH of the battery [18]. EUE can be obtained according to Eq. (7), which is the ratio between the battery capacity and module capacity. The numerator of the equation is obtained from C-rate experiments and the denominator is obtained from discharge performance at low C-rate, typically at 0.1C.

$$EUE = \frac{Battery\ capacity}{Module\ capacity} = \frac{\sum_{t0}^{to+\Delta t}(Uocv, i(t).I - Ri(t).I^2)}{\sum_{i=1}^{N} Qi.Uav} \quad (7)$$

where "*Uocv*" is the average open circuit potential, "Δt "is the discharge time, "*Uocv*,*i*(*t*)" and "*Ri*(*t*)", are the changes of *OCP* and *IR* during discharge, respectively [18].

Alternative methodologies such as voltage variation have been proposed to estimate the equalization of cells in the batteries and establish a linear correlation with SOH (see Eq. (8)) [19]. The voltage variation is more evident at low SOC (0–10 %). The high values of maximum voltage variation (ΔU_{max}) suggest a noticeable capacity loss due to poor cell equalization and, despite high SOH in individual cells, the effective SOH of modules or batteries is lower.

$$\Delta U_{max} = U_{max} - U_{min} \quad (8)$$

where "*Umax*" is the maximum voltage in the series cells and the "*Umin*" is the minimum in the series cells.

The average Fréchet distance is an artificial intelligence technique which estimates SOH by comparing experimental charge-discharge profiles with profiles under several previously collected SOH and C-rates to identify profiles with higher similarity. The average Fréchet distance diagnosis is adequate for in-operandum cells and requires a high amount of data for comparison purposes, as well as advanced software and advanced processor for data analysis [15,20]. The following criteria are applied for the characterization.

1. Two or three representative curves are selected.
2. The curves are fragmented in sections to identify the sections with higher differences.

The remanent cycle life can be estimated by coulombic efficiency analysis with ultra-high precision charger (UHPC), prolonged cycling tests under atmospheric conditions and cycling test at high temperatures to accelerate the degradation process [21,22] [14,23] The coulombic efficiency analysis is adequate for individual cells; given that is highly sensitive to experimental conditions, a rigorous standardization of chemical compositions, manufacturing conditions and environment temperature (0.1 °C) is necessary [21,22]. There are many studies reported in the literature that combine experimental data with statistical models project the remaining useful life without a long cycling test [23–26], evidencing lack of reliability of that studies. These models depend on chemistry, the morphology of active material, cells geometry, and operation conditions of the battery.

SLBs require adequate business management of diagnostic processes on modules in order to reduce dismantling and remanufacturing costs and estimate the RUL [27,28]. Although previous works implement diagnostic estimation metrologies on cells with high accuracy [29,30], for SLBs, scaling up the SOH diagnosis on modules requires a better understanding of correlation between several diagnosis techniques such as incremental capacity analyses, internal resistance changes, electrochemical impedance spectroscopy and process changes during the remaining useful life of LFP and NMC chemistries. This work aims to combine different methodologies to estimate the SOH in modules of LFP and NMC chemistry, to obtain a better understanding of SOH variation and the equalization of modules and to select the most adequate diagnosis method for each battery chemistry. In addition, a view to identifying the kinetic variations and the degradation mechanism during remaining cycle life (RUL) at several temperatures and develop a general equation for accelerated aging studies in lithium cells understanding the mechanism of cell degradation. Facing these challenges and the obtained experimental results constitute the prime novelty and the contributions of the current work. Furthermore, several alternatives such as statistical SOH distribution, Incremental capacity (IC), incremental voltage (IV) internal resistance (IR), voltage variation in series sections and electrochemical impedance spectroscopy (IV) were explored to establish diagnostic methodology accuracy and alternatives for SOH determination in second-life batteries. Additionally, a deep understanding of charge profile by the incremental capacity is achieved, with the comparison between experimental IC and calculated IC profile of LFP and NMC chemistry.

2. Experimental metodology

Two LFP EV batteries of 634 V - 9 Ah (nominal capacity of individual cell = 4.5 Ah), from an electric bus, were evaluated. The battery configuration was 192S2P (192 cells in series-2 cells in parallel), with 10 18S2P modules (59.4 V) and 1 12S2P module (39.7 V). The LFP modules were fragmented into two 9S2P semi-modules to fit to the voltage limit compliance of the multichannel equipment (60 V). The cycling test for SOH and initial SOC measured was done under constant current (CC) conditions at 9 A- 1C (2P) until reaching 31.5 V (9S), followed by OCP (5 min) and finally discharge at −9 A – 1C (2P) until reaching 22.5 V (9S).

Two NMC EV batteries of 350 V – 60 Ah (nominal capacity of individual cell = 30 Ah) from an electric vehicle with battery configuration of 96S2P, and 48 2S2P modules (7.5 V-60 Ah) of cells of 3.75 V 30 Ah were also evaluated. The cycling test for SOH and initial SOC measured was done under constant current-constant voltage charge process (CCCV) conditions, the first step at constant current of 12 A- 0.2C (2P) until reaching 8.25 V (2S), the second step at constant voltage of 8.25 V until the current was lower than 2 A (0.033C), followed by OCP (30 min) and finally discharge at −12 A – 0.2C (2P) until reaching 5 V (2S).

LFP and NMC batteries modules were tested according to battery's characteristics and following the consecutive order: 1) inspection and 3 months of storing; 2) voltage measurement of the battery and series sections to select the batteries suitable for the study; 3) discharge at 1C for LFP batteries and at 0.2C for NMC batteries to measure initial SOC; 4) 3 cycles of charge-discharge at 1C for LFP batteries and 1 initial cycle for NMC batteries at 0.2C, followed by a further 3 charge-discharge cycles after 20 days to determine the SOH; 5) voltage measurement at SOC of 100, 90, 20, 10, 0 %) to evaluate voltage variation at several SOC, IR measurement at SOC of 0, 10, 20, 30, 40, 50, 60, 70, 80, 90, 100 %; and 7) EIS Measurement at SOC of 0, 10, 20, 30, 40, 50, 60, 70, 80, 90, 100 % to evaluate the correlation of IR and electrical parameters of EIS with SOH at several SOC. Fig. 1 shows a flowchart of the performed experimental procedure.

Charge-discharge tests for SOH and SOC-initial evaluation of the modules were done in an Arbin multichannel 60 V-15 A, and the electrochemical EIS measurements were done in a SOLATRON 1470 equipment with module configurations 3S2P for LFP and 2S2P for NMC. The cell RUL was done at 1C (NMC = 30 A, LFP = 4.5 A) under temperatures of 20, 40 and 50 °C in SOLATRON 1470 equipment with a 6 V-100 A booster. The temperature was controlled in a forced convection oven BINDER KB115. Charge profile for IC analyses was smoothed by Savittzky-Golay method, 70 points 2nd order polynomial.

3. Results and discussion

3.1. SOH diagnostic

The SOH distribution of modules in the battery constitutes an alternative for studying the temperature gradient effect on capacity fading and the preferable location of modules with lower SOH [8]. Fig. S1 shows the SOH of the randomly distributed modules in LFP battery; no preferable effect of the location of the modules on the aging is observed. These results suggest the existence of an adequate heat dissipation system in the EV and indicate that a random sample is representative of SOH in the modules of battery.

Frequency distribution analysis was done to evaluate the statistical SOH distribution of modules and determine SOH of all modules in battery. The equation of normal distribution is described in Eq. (9).

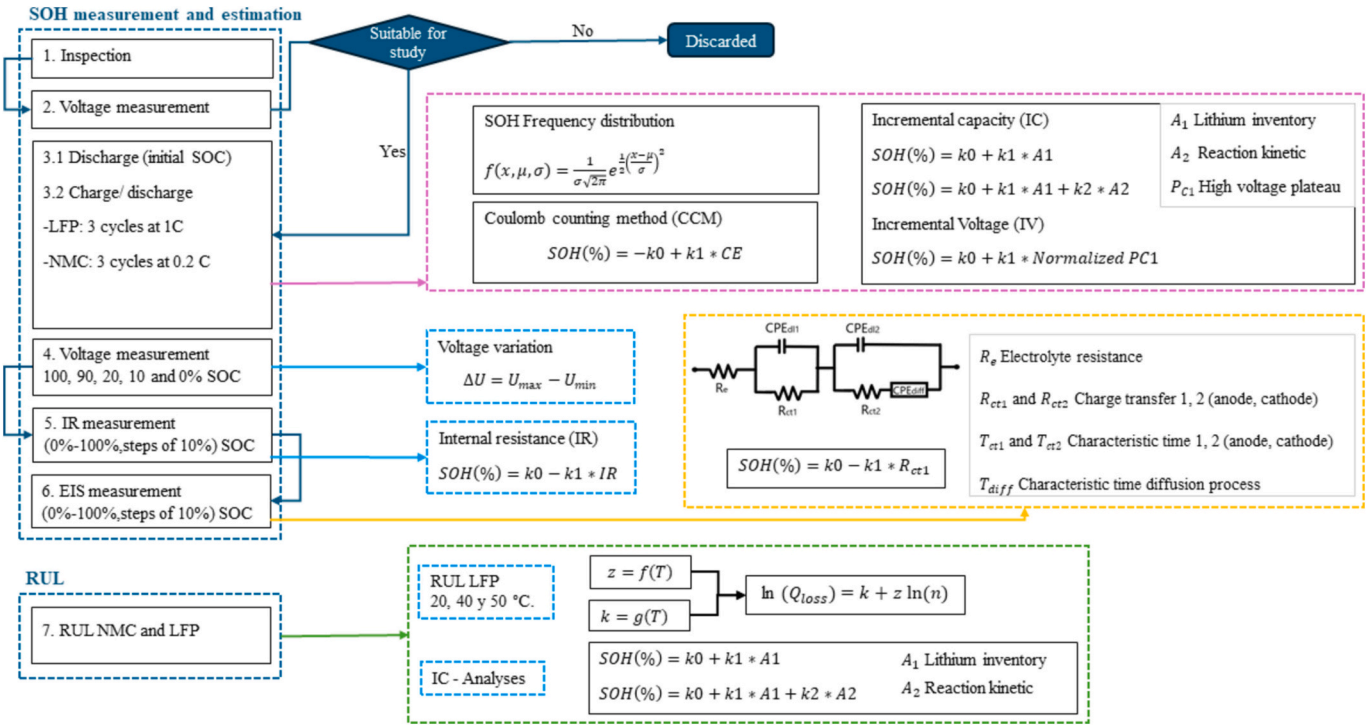

Fig. 1. Squematic flowchart of the experimental procedure.

$$f(x,\mu,\sigma)=\frac{1}{\sigma\sqrt{2\pi}}e^{-\frac{1}{2}\left(\frac{x-\mu}{\sigma}\right)^2} \tag{9}$$

where "μ" is the mean and "σ" is the standard deviation.

Fig. 2 shows the SOH frequency distribution of LFP batteries and NMC batteries. Both batteries demonstrate a normal SOH distribution with medians of 65.0 % and 60.7 %, and SOH standard deviations of 3.4 % and 2.1 % for LFP and NMC modules, respectively. These results suggest that the complete diagnosis of all modules is not required and a representative sample of them could be enough to diagnose the battery.

Other alternatives have been explored to evaluate the SOH of modules in order to study degradation mechanisms and reduce the diagnostic time. Several studies have demonstrated a linear correlation between SOH vs. voltage variation and the equalization of modules. In addition, IR increases with the capacity fading, and SOH correlation with incremental capacity (IC) and EIS parameters, and decrement of coulombs efficiency with the capacity fading has been corroborated [19].

Fig. 3a-b shows the analysis of initial SOC in order to evaluate the equalization of modules and the effect on battery SOH for LFP and NMC batteries. The results showed higher equalization than that reported by Y. Jiang et al. [8], for both chemistries. The battery capacity can be increased by 16.8 % and 15.2 % with the equalization of module in the LFP and NMC batteries, respectively. X.Li et al. estimated the equalization effect on SOH by voltage variation (ΔU) between series configurations, obtaining the highest R^2 (0.927) at SOC of 10 % [19]. The $\Delta Umax$ of a battery is measured according to Eq. (8) and the correlation with SOH was evaluated. Nevertheless, as shown in Fig. 4a-b, higher equalization than that reported by Y. Jiang et al. [8] is obtained, and SOH variation is lower in this study (64–75 %) than those reported by other authors (63.4–96.1 %) [19]. The linear relationship between ΔU and SOH shows a lower correlation, obtaining R^2 of 0.07 and 0.12 for LFP and NMC modules, respectively, see Fig. 3c, d and Fig. S2 in supporting information. These results suggest that the SOH of modules was not affected by the equalization of cells. Currently the continuous development of electronic control systems in batteries has improved the equalization systems of modules in the EV.

Incremental capacity *"IC"* (*dQ/dV*) allows the SOH of modules and degradation mechanism to be estimated. For a better understanding, *IC* was first calculated for a full-cell charge profile, starting from pristine

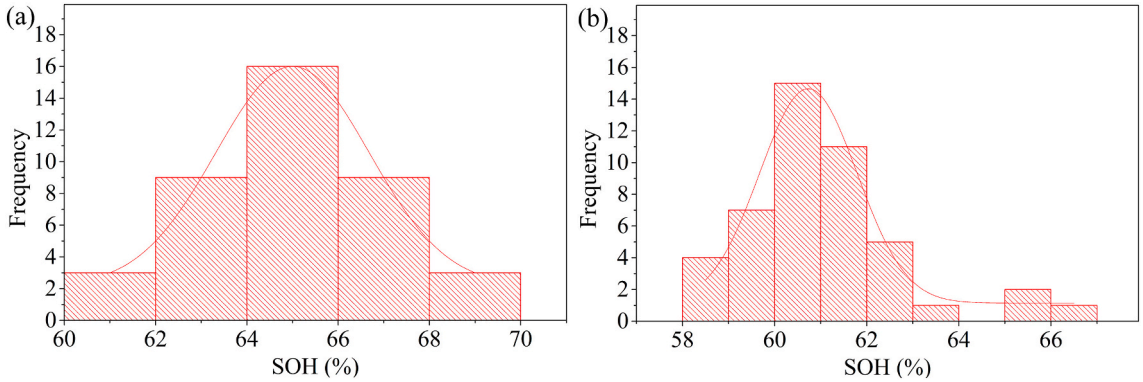

Fig. 2. SOH distribution frequencies diagram for (a) LFP modules and (b) NMC modules.

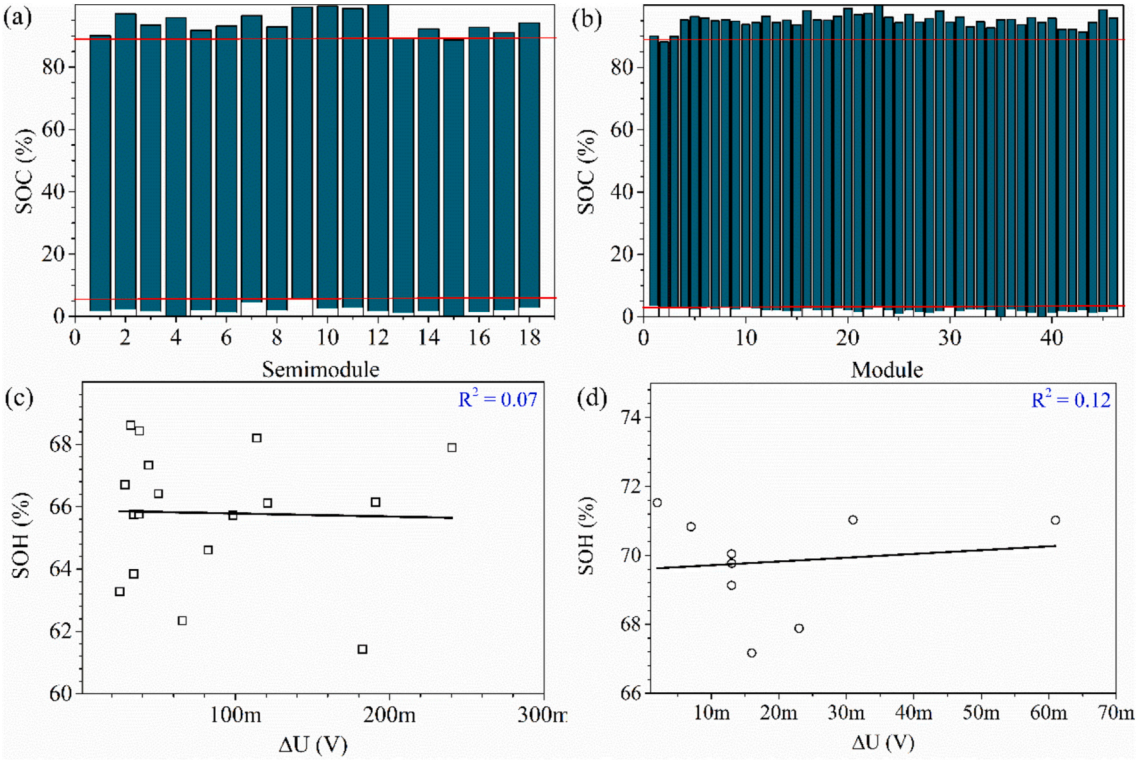

Fig. 3. (a-b) Equalizations analysis of modules for LFP and NMC batteries, respectively. (c, d) Correlation analysis between ΔU and SOH for LFP and NMC batteries, respectively.

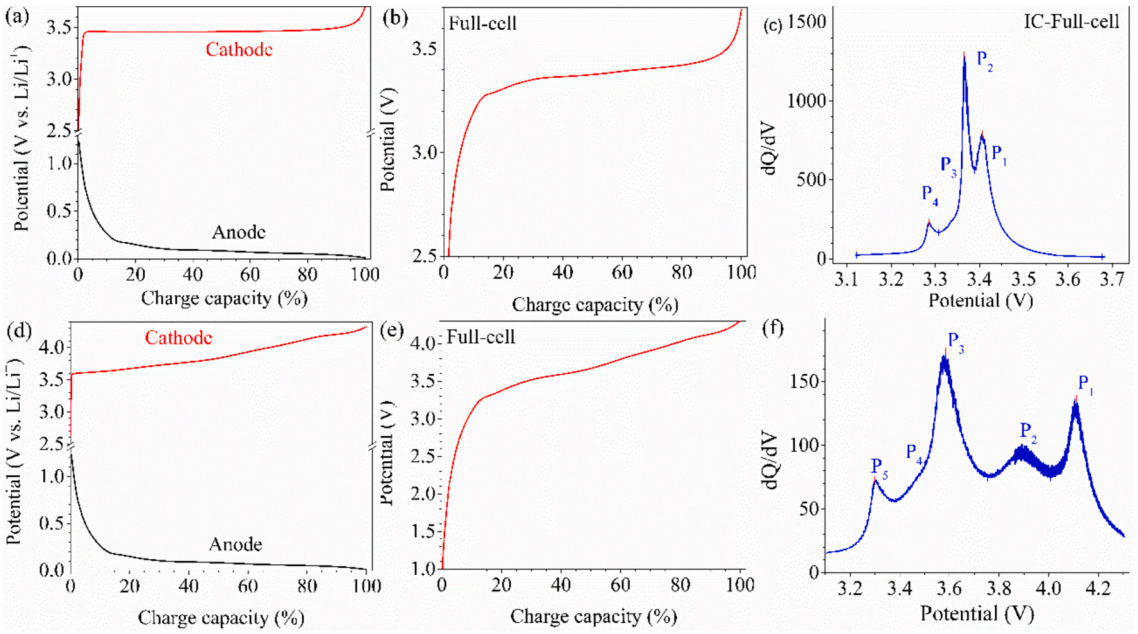

Fig. 4. Incremental capacity analysis from profiles calculated for pristine half-cells of anode and cathode of LFP and NMC batteries. (a, d) charge profile of anode and cathode half-cells. (b, e) Calculated full-cell charge profile. (c, f) IC of calculated charge profile. (a), (b), (c) correspond to LFP battery; (d), (e), (f) correspond to NMC battery.

half-cells assembled with cathode and anode as working electrodes, lithium foil as a counter and reference electrode and 1 M LiPF6- ethylene carbonate (EC): dimethyl carbonate (DMC) (1,1 *v*/v) as electrolyte. Fig. 4 (a) and (d) show the charge profile of cathode and anode half-cells of LFP and NMC chemistries, respectively. Fig. 4 (b) and (e) show the calculated charge profile for full LFP and NMC batteries. Fig. 4 (c) and (f) show the IC profile for calculated charge profiles of the full batteries.

The IC profile of the LFP cell shown in Fig. 4c displays peaks at 3.41, 3.36 and 3.28 V, named peak 1, 2 and 4, respectively and one shoulder at 3.35 V, named peak 3. Peak 1 is associated with the variation of lithium inventory, peak 2 is associated with reaction kinetics variation, and peak 4 is associated with cathode material degradation. Simultaneous

variation of peaks 1, 2, and 4 has been associated with the degradation of the active material of the anode [8]. The LFP charge profile was 46.15 % of the total area of peak 1, and when the battery degradation is affected just by lithium inventory the intercept of the correlation equation with SOH is equal to this area. The IC profile of NMC cell shown in Fig. 4f displays peaks at 4.11, 3.90, 3.58 and 3.30 V, named peaks 1, 2, 3 and 5, respectively and one shoulder at 3.50 V, named peak 4. Peak 1 is associated with the variation of lithium inventory, and peaks 3 and 5 are associated with cathode material degradation. Simultaneous variation of peaks 1, 2, 3 and 5 has been associated with the degradation of the active material of the anode. The NMC charge profile shows that the area of peak 1 in Fig. 4f is equal to 23.85 % of total charge capacity, being lower than that observed for LFP battery. Hence, if the SOH of the NMC is affected by lithium inventory, peak 1 cannot be observed at SOH lower than 76.15 %.

Fig. 5 (a) and (c) show characteristic charge profiles of LFP and NMC of used EV batteries, respectively. The voltage was normalized with the series cells number. Fig. 5 (b) and (d) show the capacity derivation concerning voltage (IC plots) for several LFP and NMC modules, for the evaluation of the variations of the voltage and peak areas. The LFP characteristic charge profile in Fig. 5a shows plateaus at 3.25 V, 3.35 V and 3.4 V; these correspond to the main peaks in the IC profile in Fig. 5b, named 4, 2 and 1, respectively. The IC plot of LFP batteries shows higher variation of peak 1, lower variation of peak 2, and no significant changes

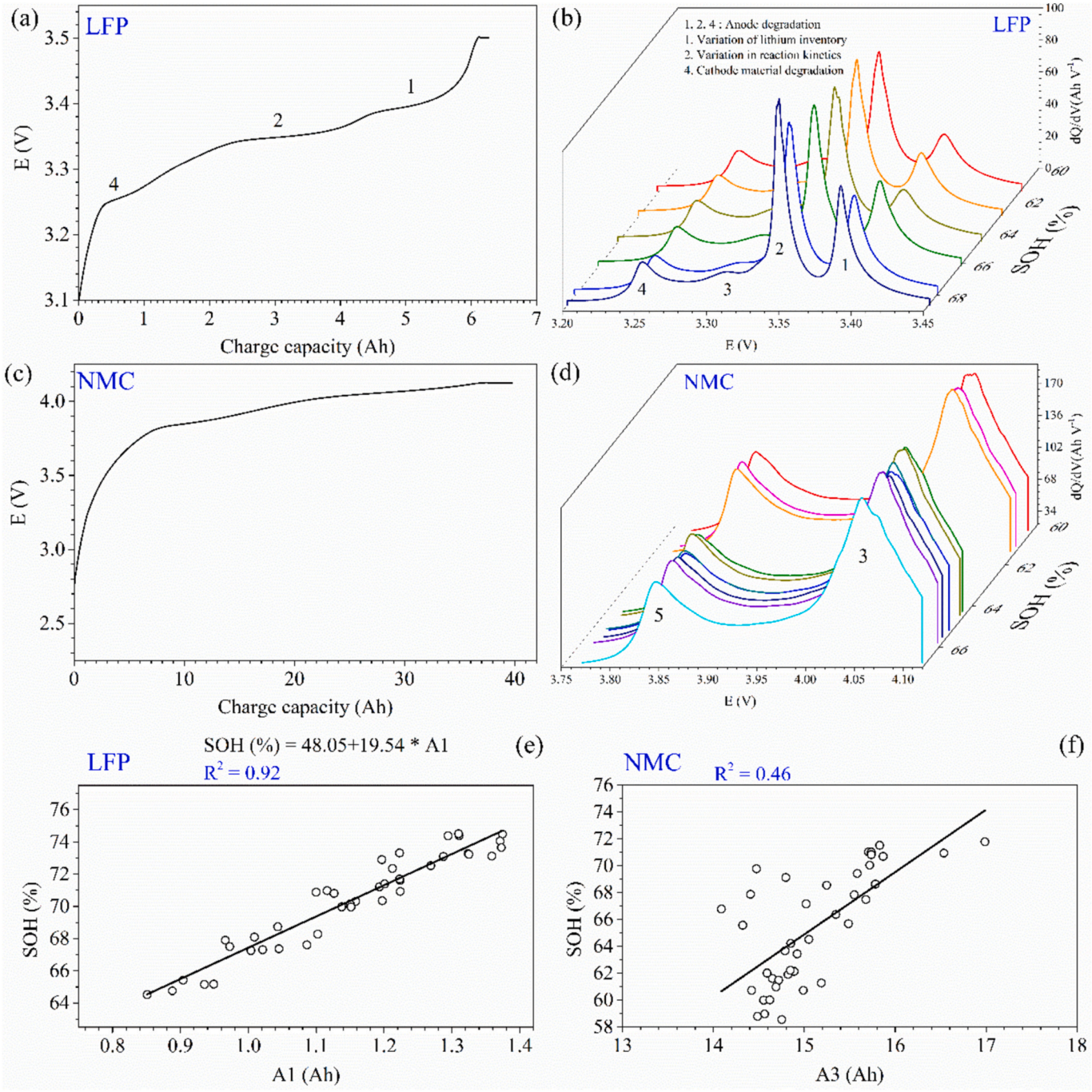

Fig. 5. (a) Characteristic LFP charge profiles at 0.5C - 20 °C. (b) Incremental capacity analysis of modules with different SOH. (c) Characteristic NMC charge profiles at 0.2C - 20 °C. (d) Incremental capacity profiles of NMC modules with different SOH. Correlation between IC-peak area 1 (A1) and SOH for (e) LFP and (f) NMC batteries.

in peak 3. The peak area 1 (A1) shows an adequate linear correlation with the battery SOH; this can be observed in Fig. 5e, which shows that the R^2 for the linear fit was 0.92. The linear fit between SOH and peak areas 1 and 2 (A1 + A2) was quite good ($R^2 = 0.99$, see Fig. S6a in the supporting information). These results indicate that correlation between SOH and IC can be improved if lithium inventory and reaction kinetic variation are included in SOH estimation by IC analyses. Experimental A1 of LFP IC profile also shows good correlation ($R^2 = 0.98$) with SOH, as can be seen in Fig. S6b in the supporting information.

NMC modules show plateaus at 3.85 V and 4.05 V in the charge profile, see Fig. 5(c). Those plateaus correspond to the peaks named 5 and 3 in the IC profile (Fig. 5(d), respectively. Additional peaks appear, given that in the NMC cathode material three oxidation processes take place at different voltages. For the NMC batteries the IC plot shows low variation of the peaks 3 and 5 with respect to SOH values. Peak areas 3 and 5 (A3, A5) show a poor correlation with the battery SOH, as can be observed in Fig. 5f ($R^2 = 0.46$) and Fig. S3a ($R^2 = 0.28$). Voltage of peaks 3 and 5 shows a low correlation with the battery SOH, as can be observed in Fig. S3b ($R^2 = 0.0.01$) and S3c ($R^2 = 0.1$) in the supporting information, respectively. The voltage shift of peak 5 was evaluated for SOH monitoring by voltage evolution, as recommended by other authors [31]. However, the SOH estimation by voltage evolution of peak 5 of the IC profile shows a poor linear correlation of $R^2 = 0.10$, as can be seen in Fig. S3c in the supporting information. These results suggest that IC analysis is not an adequate methodology to estimate the SOH of NMC modules.

Conventional IC calculation requires 3 steps to obtain the high voltage plateau capacity: i) smoothing, ii) (δQ/dV) derivative and iii) integratation of the A1 peak to calculate the peak area. Alternatively, a methodology to calculate the high voltage plateau capacity (PC1) by the second derivation of voltage with respect to capacity (δ^2V/dQ^2) can be implemented to obtain the capacity in only 2 simple steps that are simultaneously executed (smoothing and second derivation). The second derivation of voltage with respect to capacity is equal to zero ($\delta^2V/dQ^2 = 0$) at the transition between plateaus, as can be observed in Fig. 6 (a) for the LFP battery, and the magnitude between the inflections (two red points) is equal to the capacity of high voltage plateau "PC1" (peak 1 area in Fig. 6(a)). Correlation between SOH and the capacity of high voltage plateau of a LFP battery shows the same R^2 as that obtained by (δQ/dV) derivate. In addition, the normalized capacity of the high voltage plateau was calculated in order to obtain the correlation between SOH and the last plateau capacity independent of LFP cell nominal capacity, see Eq. (10). The normalized PC1 is dimensionless.

$$Normalized\ PC1 = \frac{PC1\ (Ah)}{NC\ (Ah)} \tag{10}$$

where PC1 is the capacity (Ah) of high voltage plateau and NC is the nominal capacity reported in the technical datasheet of the cell or battery. The fitting results include three LFP cells of different trademarks (100 Ah, 3.3 V), two with 100 % SOH and one with 93.3 % SOH. Fig. 6b shows excellent linear correlation ($R^2 = 0.99$) SOH and normalized PC1. The correlation equation in Fig. 6b is adequate to estimate the SOH of LFP cells with the normalized PC1 calculated from δ^2V/dQ^2 plot and the intercept of linear correlation (47.12) agreed with the intercept estimated from calculated IC profiles (46.15).

It is well known that the degradation of lithium batteries increases the resistance of electronic components and limits the kinetic and mass transport processes. The internal resistance (IR) measurement of modules and batteries allows the SOH of batteries to be estimated and can show a good correlation with coulombic efficiency (CE). The IR measurement is a low cost and fast (30–50 ms) diagnostic alternative to estimate SOH. IR value depends on ohmic resistance (electrolyte and electronic component) and on the polarization resistance (electrochemical kinetics of cell process), as was indicated in Eq. (2). The polarization resistance variation is correlated with active material degradation and with solid-electrolyte layer formation (SEI) [12]. The polarization resistance is actually SOC-dependent. Consequently, IR is also SOC-dependent, as can be evidenced in Fig. S3c. On the other hand, the ohmic resistance is not SOC-dependent. The IR - SOC dependence means that the IR diagnosis must be carried out under the same SOC in battery modules; nevertheless, the correlation also depends on the equalization degree of the cells disposed in series arrangements in the modules. For this reason, IR diagnosis requires a calibration process for each module or battery, given that in practical cases the retired batteries from vehicles arrives under a different SOC and the IR-SOC correlation can increase if diagnosis is done on individual cells. Commonly, SOH diagnosis requires complete charge and discharge processes, which take time to acheive. Fig. 7 displays the correlations of SOH-IR (65 % SOC) and SOH-CE for LFP and NMC batteries. The correlation analysis does not show good linear correlation between IR and CE for LFP modules, with values of R^2 equal to 0.04 and 0.17, respectively. Nevertheless, better correlation for NMC batteries was found, as shown in Fig. 7b, d. NMC batteries experience an acceptable linear relationship between IR and CE with SOH, with values of $R^2 = 0.76$ and 0.68, respectively. These results indicate that the chemistry of the battery influences the results of the diagnosis test. The significance of the diagnosis method and its correlation with SOH depends on the battery chemistry. It is also highlighted that IR and CE allow acceptable diagnosis of the SOH of NMC modules, while these parameters do not enable the SOH for LFP batteries to be estimated.

Kinetics parameters that influence the electrochemical performance of lithium batteries were studied by electrochemical impedance spectroscopy (EIS). EIS measurements were performed at configuration 3S2P for LFP modules and at 2S2P for NMC modules. EIS is a non-destructive technique that is sensitive to SOH and SOC, given that electronic conductivity and lithium mobility depend on vacancies, phase transitions, oxidation state and volumetric changes of the active materials present in the electrodes during the charge-discharge processes. Global SOH of modules with series or parallel cell configurations are influenced by SOC or SOH of individual cells and the electrical parameters are sometimes

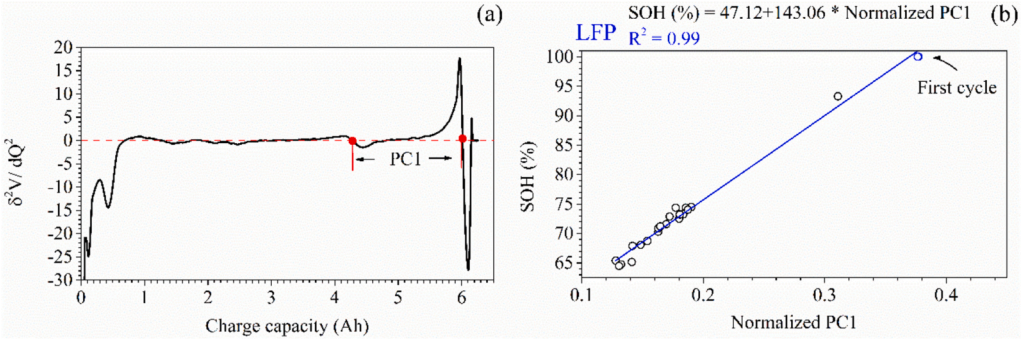

Fig. 6. (a) Second derivation of charge profile at 1C. (b) correlation between the normalized LFP high voltage plateau capacity and SOH.

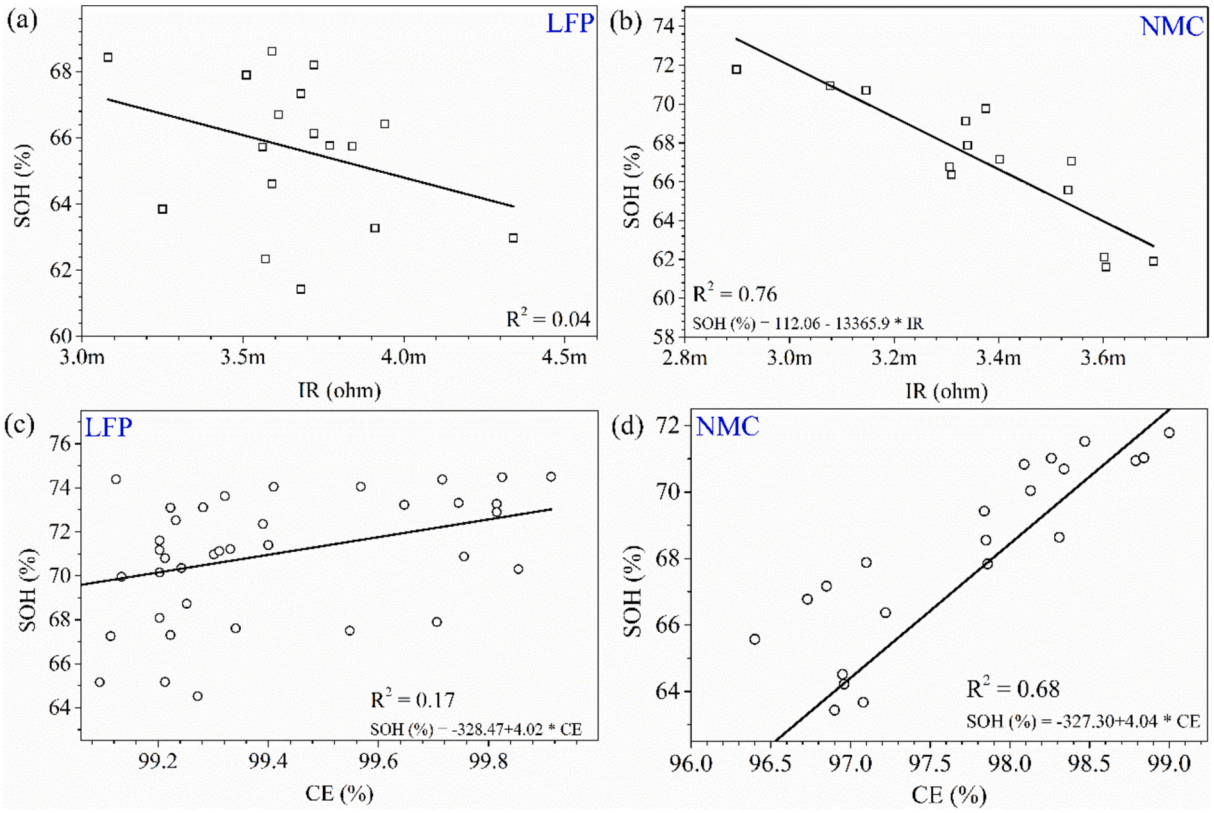

Fig. 7. (a, b) Correlation SOH-IR (65 % SOC) for LFP and NMC batteries, respectively. (c, d) Correlation SOH-Coulombic efficiency for LFP and NMC batteries, respectively.

not representative of the module's global SOH [19]. Fig. 8 shows EIS results (Nyquist plots) of LFP 3S2P modules and NMC 2S2P modules. The inductive region at high frequencies (> 0.42 kHz) in the Nyquist diagram of EIS measurements was not shown, to facilitate the EIS analysis. Two overlapping loops at high-intermediate frequencies, ~30–45 Hz for negative electrode and ~ 0.1–2.4 Hz for positive electrode, were associated with the charge transfer process in parallel with double-layer capacitance [32]. These processes were considered in series configuration in the electrical equivalent circuit shown in Fig. 8 and used to fit the experimental values of EIS measurements. The linear tail at lower frequencies (<100 mHz) associated with the diffusion process was fitted with the constant phase element (CPE) as described by Bisquert [33,34]. The intercept at high frequencies is associated with the resistance of the electrolyte and electronic part of modules. In can be seen in Fig. 8a that the charge transfer resistance of cathode material at 0 % SOC is higher than at 10 and 30 % SOC, indicating that the vacancies generated at high SOC in the cathode improve the internal conductivity of the battery. This is also true for NMC chemistry, see Fig. 8b. The comparative analysis of Nyquist plot of the EIS measurements at 0 and 10 % SOC for several sections of the LFP 3S2P modules indicates that there is no correlation between EIS and SOH (see Table S1 Fig. 8c, e). Conversely, NMC modules show increasing impendance of 3S2P with the SOC, see Fig. 8 (d) and (f). Also, the electrolyte resistance increases with SOH.

The EIS experimental results were fitted with the electrical equivalent circuit (EEC) in Fig. 8. Table S1, in the supporting information, shows the values of the electrical parameters extracted from the fit of EIS with EEC. Although several relationships were explored between SOH and the electrical parameters of EIS for LFP batteries, no good correlations were evidenced, Fig. 9a. Meanwhile, for NMC modules acceptable correlation (R^2 = 0.78) was evidenced between SOH and the charge transfer resistance of the anode/electrolyte interface (Rct1), see Fig. 9b. Additional relationships were explored between SOH and other electrical parameters of EIS (shown in Table S2) for NMC batteries, and no correlation was evidenced.

The summary of the performance and comparative correlation between LFP and NMC EV modules are shown in Table 1 for two batteries (B1 and B2). The results show similar SOH for NMC and LFP modules. The correlation analysis with several diagnostic methods demonstrates that PC1 is the most suitable method for LFP battery modules with, a correlation coefficient of 0.99 and a test time of 48 min. The other diagnostic methods show a poor correlation. On the other hand, internal resistance and Rct1 of EIS are the most suitable methods for diagnosis of the NMC modules, with R^2 values of 0.76 and 0.78 and test times of 30 min and 10 min, respectively. The other diagnostic methods show a poor correlation with the SOH. Potential variation "ΔU" in the series cells showed poor correlation with SOH, indicating that the slight SOC variation between modules (around 5 %) does not affect the capacity of the batteries. It is important to highlight that all the selected diagnosis methods with a high correlation coefficient with SOH have a lower testing time than the conventional charge-discharge method used to estimate the SOH.

Nevertheless, as shown in Fig. S4 in the supporting information, the SOH of NMC modules on cycle 1 decreases proportionally with storage time (from dismantling to diagnosis) suggesting that this effect induces errors on NMC SOH estimation by discharge capacity on cycle 1. The capacity lost during storing time was recovered after 50 cycles (11.96 ± 1.75 %) as can be observed in Fig. S4a (supporting information).

The LFP modules do not show a correlation between discharge capacity on cycle 1 and storage time before diagnosis, and the capacity recovered after 50 cycles was 1.0 ± 0.7 %. These results suggest that the diagnosis of NMC modules has to be done as fast as possible (< 15 calendar days) to improve the accuracy of SOH estimation.

Evaluated batteries show high equalization and the homogeneity of SOH suggests that statistical analyses can be done to diagnose just one representative sample of the modules of the battery. The experimental

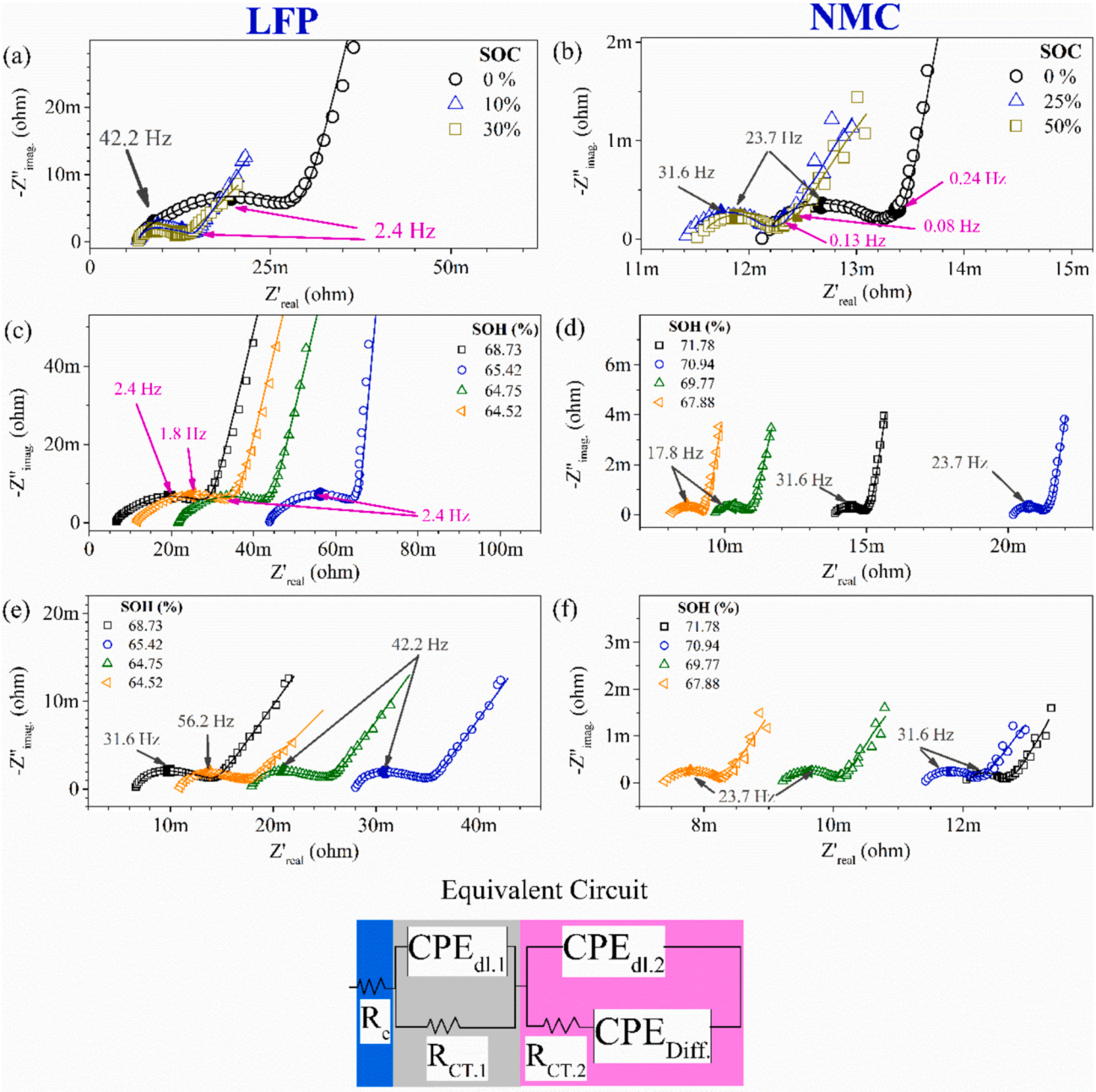

Fig. 8. EIS analysis of LFP modules 3S2P and NMC modules 2S2P (a) LFP SOC effect. (b) NMC 2S2P SOC effect (c, e) LFP SOH effect at 0 and 10 % SOC, respectively. (d, f) NMC 2S2P SOH effect at 0 and 25 % SOC. Gray frequencies (anode), Magenta frequencies (cathode). Dots experimental, line fitting. (For interpretation of the references to colour in this figure legend, the reader is referred to the web version of this article.)

equation for SOH measurement by IC shows a good agreement with IC of the calculated charge profile and good correlation ($R^2 = 0.92$). However, the degradation mechanism showed changes in lithium inventory and in the kinetics of the process. Therefore, as shown in Fig. S6a, the general equation taking into account both effects improves the correlation ($R^2 = 0.99$).

The incremental capacity for NMC chemistry showed a poor correlation with SOH due to the high number of plateaus observed in the charge profile and a general equation for estimate SOH by IC can not obtained due to variation in charge profiles of comercial cells caused by the changes in the Ni/Mn/Co ratios. NMC modules or cells showed a good correlation between SOH and the changes in charge transfer resistance on the anode/electrolyte interface (R_{ct1})-EIS ($R^2 = 0.78$) and internal resistance ($R^2 = 0.76$) done at intermediate SOC.

3.2. *Remaining useful life (RUL) for LFP and NMC batteries*

The remaining lifetime has been evaluated conventionally by long-term cycling test at 20 °C or by high temperature cycling test (30–60 °C). The last condition is commonly conducted to accelerate the degradation process of the lithium cells. Fig. 10 shows the long cycling test carried out on LFP and NMC modules at 20 °C. LFP modules, with an initial SOH of 64 %, showed high-capacity retention after 500 cycles (99 %). A slight capacity drop (2 %) after stopping the cycling process occurs; however, it is recovered in the following cycles. Meanwhile, NMC modules with an initial SOH of 70 % showed high capacity recovery during initial cycles and a high capacity retention up 360 cycles (2.2 % capacity loss), see Fig. 10b. However, after 360 cycles the capacity fell strongly and a capacity loss of 9.8 ± 4.9 % after 500 cycles was

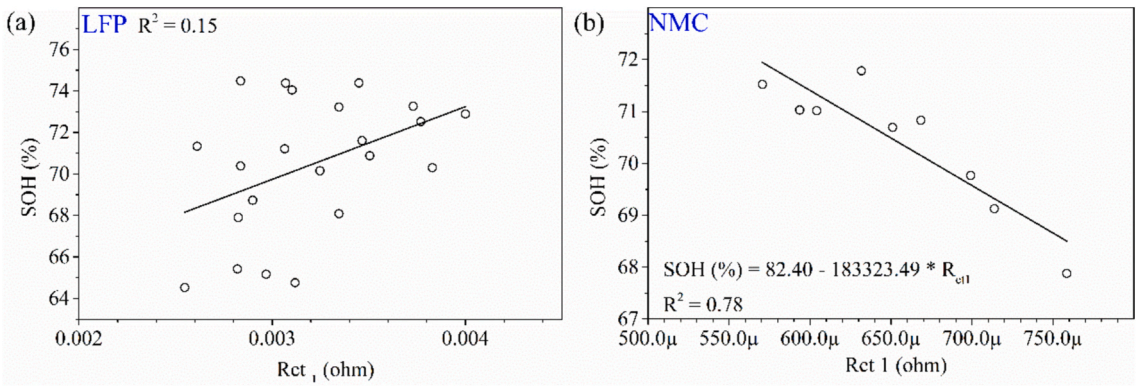

Fig. 9. (a) Correlation Rct1 – SOH for LFP modules at 10 % SOC (additional electrical parameters in supporting information Table S1) (b) Correlation Rct1-SOH for NMC modules at 25 % SOC (additional electrical parameters in supporting information Table S2).

Table 1
Performance summary of LFP EV batteries and NMC EV batteries, and correlation between diagnostic methods and SOH.

Parameter		LFP EV battery	NMC EV battery
Test time (min)		240	600
Discharge capacity (Ah)	B1	5.92 ± 0.20	36.67 ± 1.02
	B2	5.77 ± 0.15	38.78 ± 0.43
SOH (%)	B1	65.77 ± 2.23	61.11 ± 1.71
	B2	64.15 ± 1.66	64.64 ± 0.71
Test time (min)		240	240
correlation SOH-CE			
R^2		0.17	0.68
Test time (min)		1	1
correlation SOH-ΔU			
R^2		0.07	0.12
Test time (min)		48	124
correlation SOH-IC-A3			
R^2		0.92	0.51
Test time (min)		–	124
correlation SOH-IC-V-P5		–	
R^2			0.70
Test time (min)		48	–
correlation SOH-PC1			–
R^2		0.99	
Test time (ms)		30	30
correlation SOH-IR			
R^2		0.04	0.76
Test time (min)		10	10
correlation SOH-Rct		0.15	0.78
R^2			

evidenced. The lower stability and strong capacity fading of NMC modules occured because the cycling process was performed at 100 % depth of discharge (DOD), as was described by J. de Hoog et al. [35]. At high DOD, the capacity retention of NMC modules is lower than LFP batteries and the cycle life of NMC is reduced. On the other hand, when the DOD applied is moderate, i.e. around 60 %, the cycle life can be increased by around three times in NMC batteries. These results demonstrate that an adequate Battery management system (BMS) DOD control for NMC modules is required to prevent the fast capacity fading.

The LFP modules showed low capacity loss after 500 cycles (1 %). Therefore, a long cycling test or accelerated cycling test at high temperature is required to evaluate the remaining useful life (RUL) until achieving capacity loss close to 10 %. The cycle life is determined by degradation reaction kinetic ($i_{deg.}$) of the active materials present in the electrodes, which depends on the temperature and overpotential, as can be inferred by Butler Volmer Eq. (11).

$$i_{deg.} = i_0 * exp\left(-\frac{\propto n_0 F}{RT}\eta_s\right) \tag{11}$$

where, F is Faraday constant, T is the temperature, R is the ideal gas constant (8.314 J mol^{-1} K^{-1}) "i_0" is exchange current density, α is the charge transfer coefficient, "n_0" is the number of transferred electrons and η_s is the over-potential. In addition, the capacity loss "Q_{loss}" can be calculated according to Eq. (12), which is the transformation of Eq. (11). In that expression, capacity loss "Q_{loss}" is the product of the kinetic of degradation reaction "$i_{deg.}$" (Eq. (11)) and time or number of cycles "n". The factor "$\alpha n_0 F \eta_s$" is equal to Ea in Eq. (12) and exchanging current "i_0" is equivalent to "A" constant in Eq. (12). In summary, from the product of Eq. (11), number of cycles and the introduction of stress factor "z" which describes changes in degradation mechanism, an Arrhenius type

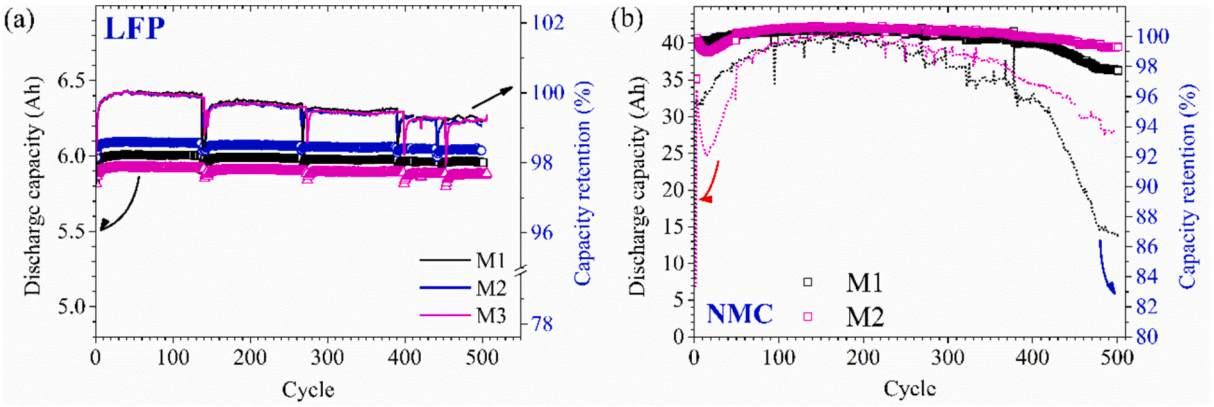

Fig. 10. Cycling test (a) LFP modules M1-M3 at 1C. (b) NMC modules M1 and M2 at 0.2C.

Eq. (12) can be obtained [36].

$$Q_{loss} = A^{*}e^{\left(\frac{-Ea}{RT}\right)}(n)^{z} \quad (12)$$

Fig. 11 shows the dependence on temperature of capacity fading of LFP modules retired from EV with an initial SOH of 66 %. The capacity retentions after 350 cycles at temperatures of 20, 40 and 50 °C were 99.5 %, 95.5 % and 12 %, respectively. As can be seen, capacity fading was accentuated at higher temperatures. At 50 °C a sudden capacity loss was observed after 230 cycles; this fast capacity fading can be associated with the local short circuit of cells. The capacity changes were studied by incremental capacity, as shown in Fig. 11b-c. Peak area 1 starts to decrease after 100 cycles at 20 and 40 °C and starts to decrease from the first cycle at 50 °C, see Fig. S5a in the supporting information. Peak area 2 increases with the cycle number at 20 and 40 °C, and at 50 °C tends to be almost stable after 100 cycles, see Fig. S5b in the supporting information. The increase in peak 2 demonstrates that cycling activates reactions involved in the charge process and this activation takes place at a lower number of cycles at 40 and 50 °C and demands more cycles at 20 °C. These results suggest that degradation products precipitate on electrodes consolidating a resistive layer that could lessen the kinetics of the charge-discharge process, affecting the battery performance. This passive layer could be released with increasing temperature or the number of charge/discharge cycles, which agrees with the suddenly capacity drop after stopping the cycling test and its recovery when the cycling test is resumed, as was shown in Fig. 10. In addition, increasing voltage in peaks 1 and 2 was evidenced, being more noticeable at 40 and 50 °C, as can be seen in Fig. S5c-d, in the supporting information.

The logarithmic form of Eq. (12) is expressed in Eq. (13), where the stress factor "*z*" is the slope and the intersect "*k*" is described by Eq. (14). Linear correlations between ln (*n-number of cycles*) vs. ln (Q_{loss}-*capacity loss on the second life used battery)* were plotted in Fig. 12a. Also, the plot between (*1/RT*) vs. (*k*) shows a linear relationship, as shown in Fig. 12 (b). The activation energy of the degradation process "*Ea*" is the slope of the line observed in Fig. 12(b), and the intersect is ln(*A*). The *Ea*, and *A* are not temperature-dependent.

$$ln\,(Q_{loss}) = ln(A) - \left(\frac{Ea}{RT}\right) + z\,ln(n) \quad (13)$$

$$k = ln(A) - \left(\frac{Ea}{RT}\right) \quad (14)$$

The fitting results of the RUL parameters (*z* and *k*) for LFP batteries at several temperatures, 100 % DOD and 1C are presented in Table 2. Stress factor "*z*" decreases with temperature (see Table 2), suggesting changes in degradation mechanism. The change in the stress factor is inversely proportional to the temperature, as described by Eq. (15) with an R^2 of 0.99 (see Fig. S7). Values of "*z*" higher than 0.5 were obtained in the current study, indicating that there are additional processes to the loss of lithium inventory involved in degradation mechanism of the cells, such as degradation of active materials [36].

$$z = 10.61 - 0.03^{*}T \quad (15)$$

According to the fitting results a general equation that describes the capacity loss of LFP batteries with temperature is proposed in Eq. (16)

$$Q_{loss} = 4.3599^{*}10^{30}{}^{*}exp\left(\frac{-198218.85}{8.314^{*}T}\right)(n)^{10.61093-0.03013^{*}T} \quad (16)$$

Remaining useful life (RUL) Eq. (16) was fitted to the experimental data of LFP batteries, and the results are shown in Fig. 13. The cycling test at 50 °C in Fig. 11a showed a severe capacity fading after 230 cycles in which the capacity loss (Q_{loss}) was 5 % (during a second life). Severe capacity fading has been associated in other studies with the short-circuit of cells caused mainly by dendrite formation promoted by the precipitation of degradation products on the anode [37–40]. The RUL at 20 °C can be estimated using Eq. (16) and assuming that the capacity loss of around 5 % is a critical value to observe short-circuit events in the cells by the dendrite formation on the anode. The RUL estimated for second-life LFP batteries at 20 °C was approximately 1200 cycles at 1C and 100 % DOD.

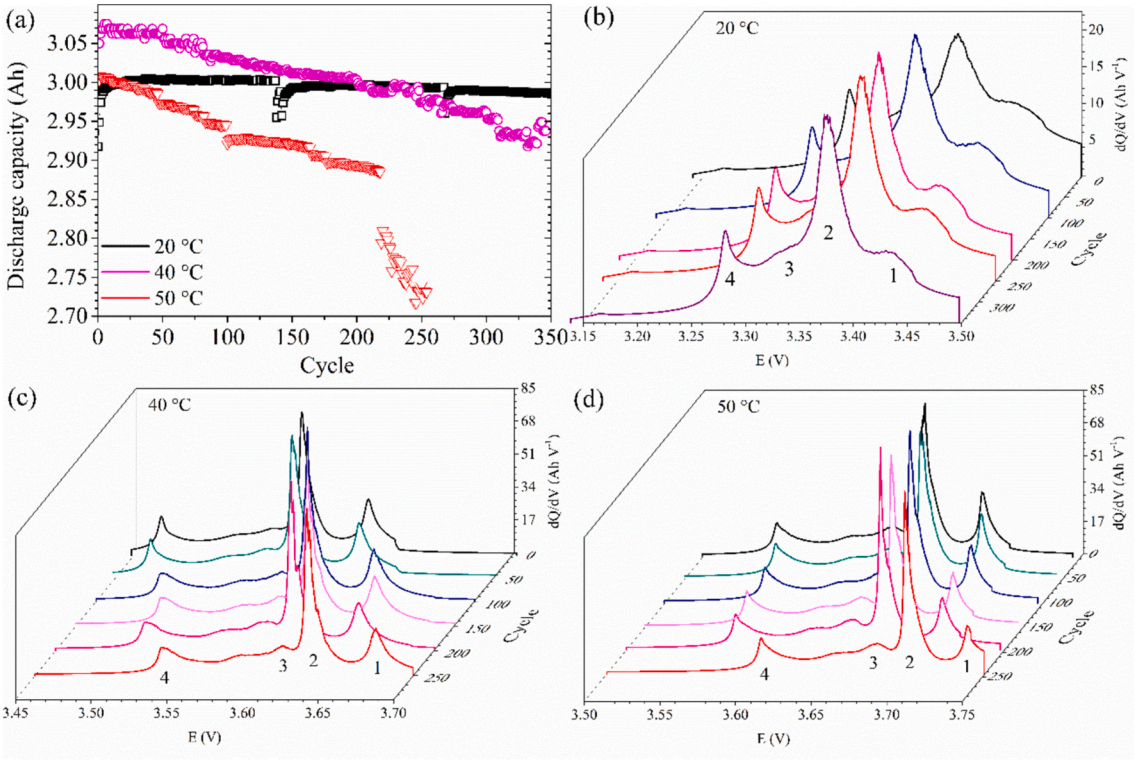

Fig. 11. (a) Cycling test of LFP batteries at several temperatures and C-rate = 1C. (b-d) Incremental capacity evolution at temperatures of 20, 40, 50 °C, respectively.

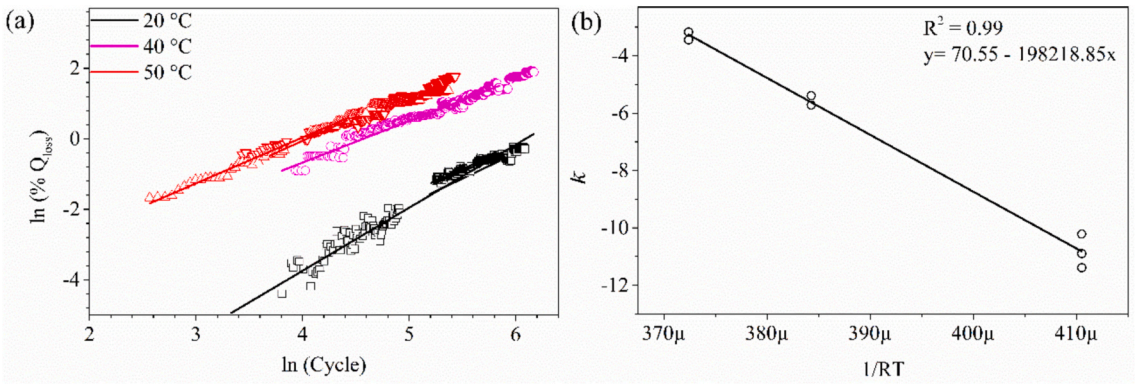

Fig. 12. (a) Logarithmic plot of Q_{loss} vs. *number of cycles* at several temperatures of LFP batteries (Linear fitting parameters in Table S4). (b) Plot of intersect (k) vs. $1/RT$.

Table 2
Fitting parameters of RUL at several temperatures, 100 % DOD and 1C.

Temperature (K)	k	z
293	−10.83 (59)	1.776 (83)
313	−5.55 (23)	1.207 (38)
323	−3.31 (19)	0.860 (42)

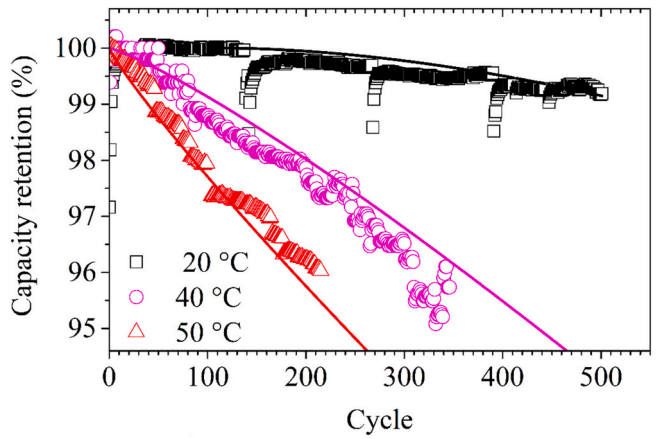

Fig. 13. Remnant lifetime estimation of LFP battery with Eq. (16), experimental data (dots), fitting (line).

4. Prospects and challenges

There are many possibilities of use SLB coming from EVs, like stationary energy storage systems, systems to support peaks or extra energy demands, support communication systems, support to security systems, etc. These alternatives contribute to circularity of the lithium-ion batteries and to solve high cost of stationary energy storage systems. However, the market of SLB has several challenges that need to be solved to promote its commercial growth, as the unknowledge of the origin of batteries that will dismantle and lack of information about first life. The adequate match between dismantled batteries and demand of SLB market. The continuous variations in configurations and chemistries developing in lithium-ion batteries implies permanent evaluation of diagnosis methodologies. The use of welding or adhesive procedures to ensambling packs of batteries increases both the cost of dismantling process and risk of damish. Battery diagnosis requires faster, low-cost and not destructive test processes, the high variation in chemistry and morphology difficult SLBs test and manufacturing standardization. The RUL information requires recalculation in real-time under the operation conditions, in order to improve the prediction life time models.

The incorporation of predictive models and artificial intelligence supported in calculated electrochemical data will bring SOH indicators and RUL protocols adaptable to the chemistry, shape and capacity variations. Advanced remote monitoring that applies and captures DC and AC signals must be used to perform data analysis of diagnostic and RUL to provide prognostic in real-time. These diagnostic and monitoring technologies can be incorporated into the first life of EVs to predict the dismantling dates. SLBs manufacturing can establish favorable first life manufacturing parameters to automate the dismantling. SLBs battery manufacturing with minimum intervention and a simple electronic reconfiguration system for adapting the battery to the voltage requirements of SLBs in the several applications.

5. Conclusion

Comparative diagnostic of lithium batteries shows differences between LFP and NMC chemical composition. Diagnostic methodologies must be based on the chemical composition of the battery. Second life batteries with suitable battery management and equalization systems guarantee homogeneous capacity loss and SOC making possible a statistical analysis to diagnose just a representative sample of modules in the battery.

SOH determination by IC shows good agreement between the equation calculated from half cells of LFP cathode-graphite anode and the linear correlation of experimental data. The incremental capacity is a promising alternative to diagnose LFP batteries. In addition, the dV/dQ allows the incremental voltage correlation to be calculated in a single step, reducing the diagnostic time from 120 min to ~40 min, and the charging process guarantees the storage of the batteries under 100 % SOH. The normalization methodology for the incremental capacity of LFP batteries allows the calculation of the SOH for cells with different capacities or shapes and the correlation between SOH and IC can be improved if lithium inventory and reaction kinetics variation are included in the SOH estimation equation by IC analyses (R^2 = 0.99), whose equation is suitable to calculate SOH in RUL studies at DOD between 70 and 100 %. The internal resistance and charge transfer resistance of EIS measurement show a good correlation with SOH for NMC batteries. However, after 70 days of rest the capacity decreases and it is completely recovered only after 50 cycles. The NMC batteries showed high capacity retention up 380 cycles at 20 °C, after 380 cycles the degradation kinetics increases and strong capacity loss of 9.8 %. at 500 cycles was evidenced. The RUL shows high stability for LFP modules, retaining >99 % of discharge capacity after 500 cycles at 20 °C and thus achieving remaining useful life higher than 5 years with retired cells from electric vehicles. There are variations in the stress factor with temperature for LFP batteries, which is consistent with kinetics and lithium inventory variation during cycle life. Incremental capacity analyses show the activation of the kinetics of the charge-discharge process

by increment of temperature and number of charge/discharge cycles. A relationship between capacity loss (Q_{loss}) and temperature was found for LFP batteries, leading to the prediction of RUL at 20 °C with good confidence.

CRediT authorship contribution statement

F.A. Vásquez: Writing – original draft, Methodology, Investigation, Formal analysis, Conceptualization. **P. Sara Gaitán:** Methodology, Investigation. **Jorge A. Calderón:** Writing – review & editing, Resources, Project administration, Funding acquisition, Conceptualization.

Author agreement statement

We the undersigned declare that this manuscript is original, has not been published before and is not currently being considered for publication elsewhere. We confirm that the manuscript has been read and approved by all named authors and that there are no other persons who satisfied the criteria for authorship but are not listed. We further confirm that the order of authors listed in the manuscript has been approved by all of us. We understand that the Corresponding Author is the sole contact for the Editorial process. They are responsible for communicating with the other authors about progress, submissions of revisions and final approval of proofs.

Declaration of competing interest

The authors declare that they have no known competing financial interests or personal relationships that could have appeared to influence the work reported in this paper.

Acknowledgements

Authors thank Colombian Ministry of Science, Technology and Innovation “Minciencias”, and the University of Antioquia for their support of the project 1115-914-91812, contract N° 119-2022.

Appendix A. Supplementary data

Supplementary data to this article can be found online at https://doi.org/10.1016/j.est.2024.114725.

Data availability

Data will be made available on request.

References

[1] MarketsandMarkets, Electric Vehicle Market. https://www.marketsandmarkets.com/Market-Reports/electric-vehicle-market-209371461.html, 2022.
[2] Andemos, Matrículas nuevas Vehículos eléctricos e híbridos, VEHÍCULOS BEV HEV PHEV, 2024.
[3] G. Avendaño, Los carros híbridos y eléctricos más vendidos en Colombia durante el 2023, MOTOR (n.d.). https://www.motor.com.co/industria/Los-carros-hibridos-y-electricos-mas-vendidos-en-Colombia-durante-2023-20240111-0002.html.
[4] D. Kamath, S. Shukla, R. Arsenault, H.C. Kim, A. Anctil, Evaluating the cost and carbon footprint of second-life electric vehicle batteries in residential and utility-level applications, Waste Manag. 113 (2020) 497–507.
[5] PowerTech, Lithium LiFePO4 vs Lead-Acid cost analysis, (n.d.). https://www.powertechsystems.eu/home/tech-corner/lithium-ion-vs-lead-acid-cost-analysis/.
[6] B. Wrålsen, R. O'Born, Use of life cycle assessment to evaluate circular economy business models in the case of Li-ion battery remanufacturing, Int. J. Life Cycle Assess. 28 (2023) 554–565.
[7] P. Eleftheriadis, S. Leva, M. Gangi, A.V. Rey, A. Borgo, G. Coslop, E. Groppo, L. Grande, M. Sedzik, Second life batteries: current regulatory framework, evaluation methods, and economic assessment: reuse, refurbish, or recycle, IEEE Ind. Appl. Mag. 30 (2024) 46–58.
[8] Y. Jiang, J. Jiang, C. Zhang, W. Zhang, Y. Gao, Q. Guo, Recognition of battery aging variations for LiFePO4 batteries in 2nd use applications combining incremental capacity analysis and statistical approaches, J. Power Sources 360 (2017) 180–188.
[9] J. Zeng, S. Liu, Research on aging mechanism and state of health prediction in lithium batteries, J. Energy Storage 72 (2023) 108274.
[10] J. Lacap, J.W. Park, L. Beslow, Development and demonstration of microgrid system utilizing second-life electric vehicle batteries, J. Energy Storage 41 (2021) 102837.
[11] A.I. Cavallo, Cell-Based Battery Modeling to Estimate the Maximum Power Flexibility for a Whole Battery Array, 2018.
[12] C. Julien, A. Mauger, A. Vijh, K. Zaghib, Lithium Batteries Science and Technology, New York, 2016.
[13] J. Meng, H. Guo, C. Niu, Y. Zhao, L. Xu, Q. Li, L. Mai, Advances in structure and property optimizations of battery electrode materials, Joule 1 (2017) 522–547.
[14] M. Broussely, S. Herreyre, P. Biensan, P. Kasztejna, K. Nechev, R.J. Staniewicz, Aging mechanism in Li ion cells and calendar life predictions, J. Power Sources 97–98 (2001) 13–21.
[15] Q. Zhang, X. Li, Z. Du, Q. Liao, Aging performance characterization and state-of-health assessment of retired lithium-ion battery modules, J. Energy Storage 40 (2021) 102743.
[16] S. Tong, J.H. Lacap, J.W. Park, Battery state of charge estimation using a load-classifying neural network, J. Energy Storage 7 (2016) 236–243.
[17] C. Weng, X. Feng, J. Sun, H. Peng, State-of-health monitoring of lithium-ion battery modules and packs via incremental capacity peak tracking, Appl. Energy 180 (2016) 360–368.
[18] Y. Jiang, J. Jiang, C. Zhang, W. Zhang, Y. Gao, C. Mi, A copula-based battery pack consistency modeling method and its application on the energy utilization efficiency estimation, Energy 189 (2019) 116219.
[19] X. Li, L. Zhang, Y. Liu, A. Pan, Q. Liao, X. Yang, A fast classification method of retired electric vehicle battery modules and their energy storage application in photovoltaic generation, Int. J. Energy Res. 44 (2020) 2337–2344.
[20] D. Jiao, H. Wang, J. Zhu, Z. Chi, S. Zeng, EV battery SOH diagnosis method based on discrete Fréchet distance, Dianli Xitong Baohu Yu Kongzhi/Power Syst. Prot. Control 44 (2016) 68–74.
[21] A.J. Smith, J.C. Burns, S. Trussler, J.R. Dahn, Precision measurements of the coulombic efficiency of lithium-ion batteries and of electrode materials for lithium-ion batteries, J. Electrochem. Soc. 157 (2010) A196.
[22] J.R. Dahn, J.C. Burns, D.A. Stevens, Importance of coulombic efficiency measurements in R & D efforts to obtain long-lived li-ion batteries, Electrochem. Soc. Interface 25 (2016) 75–78.
[23] M. Ecker, J.B. Gerschler, J. Vogel, S. Käbitz, F. Hust, P. Dechent, D.U. Sauer, Development of a lifetime prediction model for lithium-ion batteries based on extended accelerated aging test data, J. Power Sources 215 (2012) 248–257.
[24] Q. Xia, D. Yang, Z. Wang, Y. Ren, B. Sun, Q. Feng, C. Qian, Multiphysical modeling for life analysis of lithium-ion battery pack in electric vehicles, Renew. Sustain. Energy Rev. 131 (2020) 109993.
[25] Y. Zhang, Z. Peng, Y. Guan, L. Wu, Prognostics of battery cycle life in the early-cycle stage based on hybrid model, Energy 221 (2021) 119901.
[26] L. Deng, W. Shen, H. Wang, S. Wang, A rest-time-based prognostic model for remaining useful life prediction of lithium-ion battery, Neural Comput. & Applic. 33 (2021) 2035–2046.
[27] C.A. Rufino Júnior, E. Riva Sanseverino, P. Gallo, D. Koch, Y. Kotak, H. G. Schweiger, H. Zanin, Towards a business model for second-life batteries – barriers, opportunities, uncertainties, and technologies, J. Energy Chem. 78 (2023) 507–525.
[28] H. Iqbal, S. Sarwar, D. Kirli, J.K.H. Shek, A.E. Kiprakis, A survey of second-life batteries based on techno-economic perspective and applications-based analysis, Carbon Neutrality 2 (2023).
[29] J.A. Braun, R. Behmann, D. Chabrol, F. Fuchs, W.G. Bessler, Single-cell operando SOC and SOH diagnosis in a 24 V lithium iron phosphate battery with a voltage-controlled model, J. Energy Storage 85 (2024).
[30] M. Faraji-Niri, M. Rashid, J. Sansom, M. Sheikh, D. Widanage, J. Marco, Accelerated state of health estimation of second life lithium-ion batteries via electrochemical impedance spectroscopy tests and machine learning techniques, J. Energy Storage 58 (2023) 106295.
[31] D.I. Stroe, E. Schaltz, SOH estimation of LMO/NMC-based electric vehicle lithium-ion batteries using the incremental capacity analysis technique, 2018 IEEE energy convers, Congr. Expo. ECCE 2018 (2018) 2720–2725.
[32] I.J. Gordon, S. Genies, G. Si Larbi, A. Boulineau, L. Daniel, M. Alias, Original implementation of Electrochemical Impedance Spectroscopy (EIS) in symmetric cells: evaluation of post-mortem protocols applied to characterize electrode materials for Li-ion batteries, J. Power Sources 307 (2016) 788–795.
[33] J. Bisquert, G. Garcia-Belmonte, F. Fabregat-Santiago, P.R. Bueno, Theoretical models for ac impedance of finite diffusion layers exhibiting low frequency dispersion, J. Electroanal. Chem. 475 (1999) 152–163.
[34] J. Bisquert, G. Garcia-belmonte, P. Bueno, E. Longo, L.O. Bulhoes, Impedance of constant phase element (CPE) -blocked diffusion in film electrodes, J. Electroanal. Chem. 452 (1998) 229–234.
[35] J. de Hoog, J.M. Timmermans, D. Ioan-Stroe, M. Swierczynski, J. Jaguemont, S. Goutam, N. Omar, J. Van Mierlo, P. Van Den Bossche, Combined cycling and calendar capacity fade modeling of a nickel-manganese-cobalt oxide cell with real-life profile validation, Appl. Energy 200 (2017) 47–61.
[36] J. Wang, P. Liu, J. Hicks-Garner, E. Sherman, S. Soukiazian, M. Verbrugge, H. Tataria, J. Musser, P. Finamore, Cycle-life model for graphite-LiFePO4 cells, J. Power Sources 196 (2011) 3942–3948.
[37] F.A. Vásquez, N.C. Rosero-Navarro, R. Jalem, A. Miura, Y. Goto, Y. Tateyama, J. A. Calderón, K. Tadanaga, Microwave assisted preparation of LiFePO4/C coated LiMn1.6Ni0.4O4 for Li-ion batteries with superior electrochemical properties, Appl. Mater. Today 30 (2023).

[38] X. Han, L. Lu, Y. Zheng, X. Feng, Z. Li, J. Li, M. Ouyang, A review on the key issues of the lithium ion battery degradation among the whole life cycle, ETransportation 1 (2019) 100005.
[39] T.-F. Yi, J. Mei, Y.-R. Zhu, Key strategies for enhancing the cycling stability and rate capacity of LiNi0.5Mn1.5O4 as high-voltage cathode materials for high power lithium-ion batteries, J. Power Sources 316 (2016) 85–105.
[40] Y. Hua, S. Zhou, Y. Huang, X. Liu, H. Ling, X. Zhou, C. Zhang, S. Yang, Sustainable value chain of retired lithium-ion batteries for electric vehicles, J. Power Sources 478 (2020) 228753.